Contrib. Astron. Obs. Skalnaté Pleso **56/3**, 35 – 53, (2026)
https://doi.org/10.31577/caosp.2026.56.3.35

A Gaia DR3–LAMOST reassessment of high-velocity star candidates with geometric-distance-aware kinematics

F. Li[1], **G. Huang**[2] **and L. Yang**[3]

[1] *School of Artificial Intelligence, Nanjing Vocational College of Information Technology, Nanjing, China (E-mail: liff@njcit.cn) (corresponding author)*

[2] *College of Information Engineering, Northwest A&F University, Yangling, China (E-mail: harry.huang@nwafu.edu.cn)*

[3] *College of Applied Technology, Nanjing University of Information Science and Technology, Nanjing, China (E-mail: 190302282228@csit.edu.cn)*

Received: May 1, 2026; Accepted: May 20, 2026

Abstract. We revisit three published high-velocity-star catalogues drawn from Gaia and LAMOST – Li et al. (2021, 591 stars), Li et al. (2023, 88 stars) and Liao et al. (2024, 519 stars) – and quantify how the published unbound classification of these candidates changes with the choice of distance estimator and with the choice of radial-velocity catalogue. After Gaia DR3 source_id resolution and de-duplication our master sample contains 1101 unique stars. 675 of them satisfy ruwe < 1.4, $\varpi/\sigma_\varpi > 5$ and carry a Gaia DR3 radial velocity (the Gaia-only clean sample). 356 additionally pass a 1 arcsec LAMOST DR9 LRS cross-match, atmospheric-parameter cuts and a $50\,\mathrm{km\,s^{-1}}$ Gaia–LAMOST RV agreement test (the final-strict sample). For every star in this strict subset, the three-dimensional Galactocentric rest-frame speed $v_{\rm grf}$ and the local escape speed $v_{\rm esc}$ are computed with a 1000-draw Monte Carlo under the MWPotential2014 potential of Bovy (2015), once with inverse-parallax distances ($1000/\varpi$) and once with the geometric distances of Bailer-Jones et al. (2021). Switching from inverse parallax to Bailer-Jones distances on the same 356 stars reduces the count with $P_{\rm unbound} = P(v_{\rm grf} > v_{\rm esc}) > 0.5$ from **48 to 3**, and the count with $P_{\rm unbound} > 0.9$ from **12 to 1**; 45 stars are downgraded across the $P_{\rm unbound} = 0.5$ threshold and none are gained. Substituting LAMOST radial velocities for Gaia radial velocities on the same subset changes the median $v_{\rm grf}$ by $0.00\,\mathrm{km\,s^{-1}}$ ($p_{90}|\Delta v_{\rm grf}| = 5.7\,\mathrm{km\,s^{-1}}$) and flips the $P_{\rm unbound} = 0.5$ classification of one star out of 356. The unbound classification of these published candidates is therefore set by the distance estimator, not by the choice of radial-velocity catalogue. The final-strict sample, a Top-15 main candidate table, and a Top-30 machine-readable supplementary CSV are released with this paper; the three highest-confidence candidates are metal-poor giants that warrant targeted spectroscopic follow-up.

[1] F. Li and G. Huang contributed equally to this work. Correspondence and material requests should be addressed to F. Li ((E-mail: liff@njcit.cn)).

Key words: high-velocity stars – Galaxy: kinematics and dynamics – stars: distances – catalogues – methods: data analysis

1. Introduction

High-velocity stars (HVS) trace the most extreme end of Galactic stellar kinematics. The classical picture of Hills (1988) predicts that tidal disruption of close binaries by the central massive black hole ejects stars at speeds well above the local Galactic escape speed; this mechanism was placed on a firm theoretical footing by Yu & Tremaine (2003) and observationally established by Brown et al. (2005), who reported the first unbound HVS in the Milky Way halo. The subsequent decade-and-a-half of dedicated surveys (Brown et al., 2007; Kenyon et al., 2008; Brown et al., 2014, and references therein) consolidated HVSs as a distinct dynamical class, reviewed comprehensively by Brown (2015).

The advent of Gaia astrometry transformed the HVS landscape. Both Boubert et al. (2018) and Marchetti et al. (2019) revisited literature HVS catalogues using Gaia DR2 phase-space information and showed that the published unbound classification of many candidates depended sensitively on the assumed distance scale and on the propagation of parallax uncertainties. The combination of Gaia DR3 with LAMOST DR9 (Cui et al., 2012; Yan et al., 2022) now provides 6D phase-space coverage with self-consistent atmospheric parameters for a substantial fraction of bright candidates, and three recent VizieR-published catalogues (Li et al., 2021, 2023; Liao et al., 2024) compile a combined 1198 candidate rows that are the natural starting point for any contemporary reassessment.

The interpretation of these candidates as bound or unbound, however, hinges on the choice of distance estimator. Inverse parallax, $1/\varpi$, is biased toward larger distances and increased random errors precisely in the high-velocity regime where parallax signal-to-noise is small (Bailer-Jones, 2015; Luri et al., 2018; Lindegren et al., 2021). The geometric-distance catalogue of Bailer-Jones et al. (2021), which folds in a Galactic prior, returns systematically smaller distances for parallax-uncertain stars and is now the standard product for kinematic work.

In this paper the unbound classification of the three published catalogues is re-derived under both distance estimators, with uncertainties propagated through a 1000-draw Monte Carlo sampler, and the robustness of the conclusion is tested against the choice of radial-velocity catalogue (Gaia DR3 vs. LAMOST DR9). The comparison is carried out on the final-strict sample of 356 stars defined in Section 2.4, so that the inverse-parallax and Bailer-Jones passes share identical proper motions, radial velocities, LAMOST-quality cuts and Monte Carlo error budgets. Any change in the unbound count then reflects the distance estimator alone. For this fixed subset, $P_{\rm unbound} > 0.5$ falls from 48 to 3 and $P_{\rm unbound} > 0.9$ falls from 12 to 1 between the two distance choices. The radial-velocity catalogue has almost no effect: the median $v_{\rm grf}$ shifts by $0\,{\rm km\,s^{-1}}$ ($p_{90}|\Delta v_{\rm grf}| = 5.7\,{\rm km\,s^{-1}}$).

The unbound classification of the published candidates is therefore set by the distance estimator.

The present work is complementary to the recent CAOSP study by Elsanhoury (2025), which used a similar combination of Gaia DR3 and LAMOST DR9 high-velocity-star catalogues to derive Galactic kinematic parameters: velocity ellipsoids, the solar motion and the Oort constants. The questions are different. The U, V, W statistics and the Oort constants are not recomputed here, and no new candidate sample is reported. Instead, the three published catalogues, the cross-match and the quality cuts are kept fixed, and the analysis isolates a single methodological choice: the distance estimator that enters the unbound probability. Elsanhoury (2025) characterises the kinematic distribution of high-velocity stars; the present analysis characterises the sensitivity of their unbound classification to the distance prescription.

The paper is organised as follows. Section 2 describes the sample construction. Section 3 details the kinematic methods, Bailer-Jones distance upgrade, and the Monte Carlo error propagation. Section 4 presents the results, anchored on seven figures and three tables. Section 5 discusses the distance-driven downgrade, the physical context of the surviving Top-3 candidates, and the limitations of the analysis. Section 6 concludes.

2. Data and sample construction

2.1. Source catalogues

Three published high-velocity-star candidate catalogues serve as input. All of them are available through VizieR (Ochsenbein et al., 2000) and downloaded with ASTROQUERY (Ginsburg et al., 2019):

- **li2021**: `J/ApJS/252/3/hivelscs`, the Li et al. (2021) catalogue of 591 high-velocity-star candidates selected from LAMOST DR7 and Gaia DR2.
- **li2023**: `J/AJ/166/12/table5`, the 88-row Table A1 of Li et al. (2023); we deliberately use the full Table A1 rather than the 52-row escape-velocity-filtered subset (`table2`) as our parent sample.
- **liao2024**: `J/AJ/167/76/table6`, the 519-star catalogue of Liao et al. (2024) that incorporates the gravitational impact of the Large Magellanic Cloud.

The combined raw input is 1198 catalogue rows.

2.2. Gaia DR3 enrichment

For every catalogue source we resolve the Gaia DR3 source_id via VizieR and run an asynchronous TAP upload-join against `gaiadr3.gaia_source` (Gaia Collaboration et al., 2023) to retrieve `parallax`, `parallax_error`, $\mu_{\alpha*}$, μ_δ and their errors, the Gaia radial velocity `radial_velocity` with its error, `phot_g_mean_mag`,

`phot_bp_mean_mag`, `phot_rp_mean_mag`, and `ruwe`. Ten of the 591 li2021 source_ids do not resolve in DR3 (merged or removed between EDR3 and DR3). Combined across the three catalogues, we obtain 1188 successful Gaia DR3 matches; deduplication across catalogues yields 1101 unique source_ids that constitute the master sample.

2.3. LAMOST DR9 cross-match

The public LAMOST DR9 LRS stellar parameter catalogue, containing 6 921 466 rows after sentinel-value cleanup, is adopted for the cross-match. Atmospheric parameters and radial velocities are produced by the LSP3 pipeline (Xiang et al., 2015); the survey design and decadal status are described in Zhao et al. (2012); Deng et al. (2012); Yan et al. (2022). Cross-matching the 1101 master sources against this catalogue with `astropy.coordinates.SkyCoord` (Astropy Collaboration et al., 2013, 2018) at 1 arcsec yields 928 Gaia–LAMOST pairs (multi-epoch) and 651 unique Gaia sources matched. For multi-epoch matches we retain the highest-snrg record per Gaia source. The full angular separation distribution has median 0.31 arcsec and 99% percentile 0.91 arcsec, well within the match radius.

2.4. Quality cuts and analysis samples

We define the following Boolean flags (motivated by Lindegren et al., 2021; Luri et al., 2018):

- `q_gaia_astrometry`: ruwe < 1.4 AND $\varpi > 0$ AND $\varpi/\sigma_\varpi > 5$.
- `q_gaia_rv`: Gaia DR3 radial velocity available.
- `q_lamost`: 1 arcsec LAMOST cross-match success.
- `q_lamost_quality`: `q_lamost` AND $T_{\rm eff}$, $\log g$, [Fe/H] all reported AND continuum $S/N \geq 20$.
- `q_rv_consistent`: both Gaia and LAMOST RV reported, $|\Delta v_{\rm RV}| \leq 50\,{\rm km\,s^{-1}}$.

Two analysis populations follow from these flags. The *Gaia-only clean* sample is the conjunction of `q_gaia_astrometry` and `q_gaia_rv` (N=675), used as the kinematic background. The *final strict* sample additionally requires `q_lamost_quality` and `q_rv_consistent` (N=356), and forms the population on which all candidate statistics are based. Two stars exceed the $|\Delta v_{\rm RV}| > 50\,{\rm km\,s^{-1}}$ threshold but otherwise satisfy every gate; they are kept in the master table and exported separately as RV-outlier follow-up candidates rather than included in the final strict subset.

The full sample-construction funnel is shown in Fig. 1 and tabulated in Table 1.

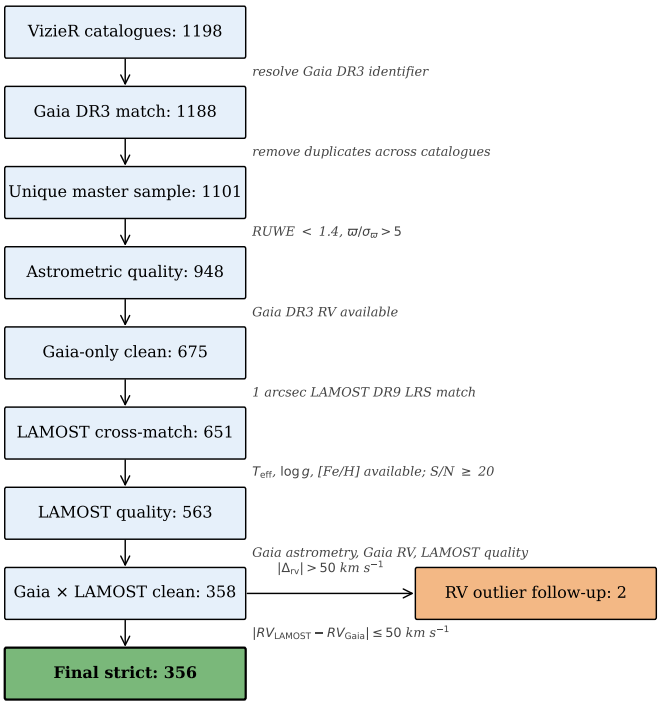

Figure 1. Sample construction. The vertical chain shows the row count after each filter, with the gate criterion annotated to the right of the arrows. The final-strict analysis sample (356 stars; dark green) is the population used for the Top-30 candidate table; the RV-outlier follow-up subset (2 stars; orange side branch) is reported separately and is not part of the final-strict sample.

3. Methods

3.1. Coordinate frame and solar parameters

All kinematic quantities are computed in the Galactocentric frame implemented in `astropy.coordinates` (Astropy Collaboration et al., 2013, 2018). We adopt $R_\odot = 8.122\,\mathrm{kpc}$ (Gravity Collaboration et al., 2018), $z_\odot = 0.0208\,\mathrm{kpc}$ (Bennett & Bovy, 2019), and a solar Galactocentric Cartesian velocity of $(12.9, 245.6, 7.78)\,\mathrm{km\,s^{-1}}$, drawn from Reid & Brunthaler (2020) for the absolute

Table 1. Sample construction and quality cuts.

Stage	N	Definition
VizieR rows	1198	All three high-velocity-star catalogues.
Gaia DR3 hit	1188	VizieR `Gaia` ids that resolve in `gaiadr3.gaia_source`.
Unique Gaia source_id (master)	1101	After de-duplication across catalogues.
`q_gaia_astrometry`	948	RUWE < 1.4 and $\varpi > 0$ and $\varpi/\sigma_\varpi > 5$.
Gaia-only clean	675	`q_gaia_astrometry` and Gaia RV available.
Gaia × LAMOST matched	651	1 arcsec sky cross-match (any quality).
`q_lamost_quality`	563	LAMOST $T_{\rm eff}$, $\log g$, [Fe/H] all reported and SNR ≥ 20.
Gaia × LAMOST clean	358	`q_gaia_astrometry` and Gaia RV and `q_lamost_quality`.
Final strict	356	Above and $\lvert v_{\rm RV,LAMOST} - v_{\rm RV,Gaia}\rvert \leq 50\,{\rm km\,s^{-1}}$.
RV-outlier follow-up	2	Above gates and $\lvert\Delta v_{\rm RV}\rvert > 50\,{\rm km\,s^{-1}}$; reported separately.

component and from Schönrich et al. (2010) for the local peculiar component.

The (U, V, W) components reported in Fig. 4 and the supplementary Top-30 CSV are heliocentric Galactic Cartesian, with U positive toward the Galactic centre, V positive in the direction of Galactic rotation, and W positive toward the North Galactic Pole; they are not LSR-corrected. The Galactocentric speed $v_{\rm grf}$ and the planar local escape speed $v_{\rm esc}(R_{\rm gc})$ are evaluated under MWPotential2014 (Bovy, 2015); alternative potentials of comparable parameter quality (McMillan, 2017; Piffl et al., 2014; Monari et al., 2018) change $v_{\rm esc}(R_\odot)$ at the few-percent level and are folded into the discussion of systematics in Sect. 5.4.

3.2. Distance estimators

Two distance estimators are compared. The *preliminary* distance is the inverse-parallax distance $d_\varpi = 1000/\varpi\,{\rm pc}$, with the well-known biases for parallax-uncertain stars (Bailer-Jones, 2015; Luri et al., 2018). The *primary* distance is the Bailer-Jones geometric distance $r_{\rm med,geo}$ from Bailer-Jones et al. (2021), queried as the `r_med_geo` column of the `external.gaiaedr3_distance` table on the Gaia archive; we also retrieve the 16th and 84th percentiles $r_{\rm lo,geo}$ and $r_{\rm hi,geo}$ for Monte Carlo sampling. All 1101 master sources match the Bailer-Jones catalogue successfully; EDR3↔DR3 source_id compatibility is 100% in our sample. Figure 3 compares the two estimators directly and is discussed in Sect. 4.2.

3.3. Monte Carlo error propagation

For each star we draw $N_{\rm MC} = 1000$ jointly sampled realizations of (ϖ *or* $r_{\rm med,geo}$), $\mu_{\alpha*}$, μ_δ, and the adopted radial velocity. Distances under the inverse-parallax pass are sampled from a normal $\mathcal{N}(\varpi, \sigma_\varpi)$ truncated at $\varpi > 0$. Distances under the BJ pass are sampled log-normally with $\sigma_{\log d} = (\log_{10} r_{\rm hi,geo} - \log_{10} r_{\rm lo,geo})/2$ to handle the typical asymmetry of the BJ percentiles. Proper motions and RV are sampled from independent normals with their reported errors. For each draw we compute (U, V, W), $v_{\rm grf}$, $V_{\rm tot,helio}$, the local escape speed $v_{\rm esc}(R_{\rm gc})$, and the ratio $v_{\rm grf}/v_{\rm esc}$; the unbound probability is the MC fraction with $v_{\rm grf} > v_{\rm esc}$.

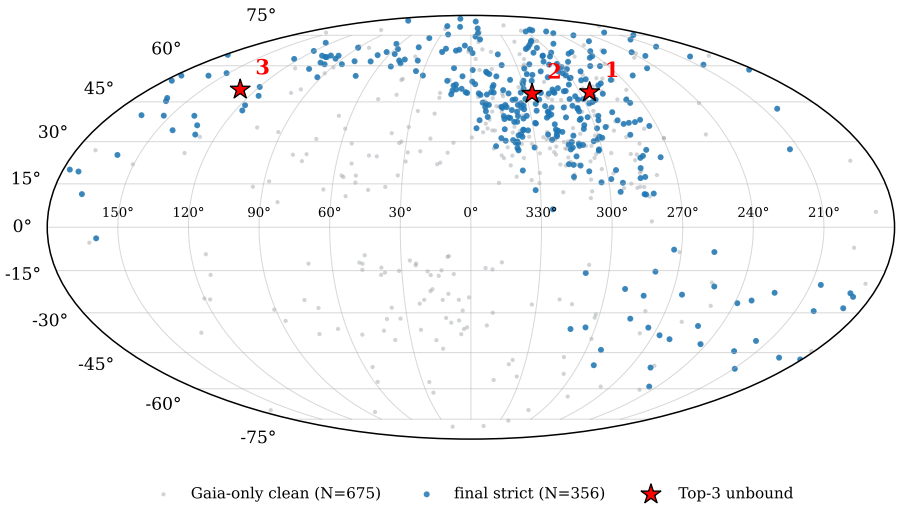

Figure 2. Galactic sky distribution of the Gaia-only clean background (grey), the final-strict sample (blue) and the three highest-confidence unbound candidates (red stars, labelled 1–3). Catalogue provenance is not encoded by colour to keep the figure legible.

3.4. Radial-velocity sensitivity check

On the final-strict sample we re-run the kinematic solution with the LAMOST radial velocity replacing the Gaia DR3 value, keeping every other input identical. We label the two resulting estimates $v_{\rm grf}^{\rm Gaia}$ and $v_{\rm grf}^{\rm LAMOST}$; their per-star difference $\Delta v_{\rm grf} = v_{\rm grf}^{\rm LAMOST} - v_{\rm grf}^{\rm Gaia}$ underpins Sect. 4.5 and Fig. 7.

4. Results

4.1. Sky distribution

Figure 2 shows the Galactic-coordinate distribution of the 675 Gaia-only-clean sources (light grey), the 356 final-strict sources (blue) and the three highest-confidence unbound candidates (red stars). The footprint is dominated by the LAMOST-accessible northern declinations, with a strong concentration above the Galactic plane consistent with halo-tracer kinematics. The 88-star Li et al. (2023) subset is retained in the Gaia-only analysis but contributes no objects to the final-strict sample under our LAMOST cross-match and quality criteria; conclusions involving atmospheric parameters are therefore based primarily on the Li et al. (2021) and Liao et al. (2024) subsets.

Table 2. Distance and kinematic sensitivity summary. All counts are computed on the same 356-star final-strict sample; the two columns differ only in the distance estimator.

Quantity	Inverse parallax	Bailer–Jones
Sample size	356	356
$P_{\rm unbound} > 0.5$	48	3
$P_{\rm unbound} > 0.7$	29	1
$P_{\rm unbound} > 0.9$	12	1
Stars downgraded across $P = 0.5$	—	45
Stars promoted across $P = 0.5$	—	0
Median $r_{\rm med,geo}/(1000/\varpi)$	—	0.88

4.2. Distance reassessment

Figure 3 compares inverse-parallax and Bailer-Jones distances on the master sample. Bailer-Jones distances are systematically smaller, with median $r_{\rm med,geo}/(1000/\varpi) = 0.88$ across the master sample and 0.76 on the 50 candidates with the largest preliminary $P_{\rm unbound}$ (red triangles). For tangentially-dominated objects the implied total peculiar speed scales linearly with distance; the 24% distance shrinkage on the Top-50 therefore translates directly into a $\sim$ 24% reduction in $v_{\rm grf}$, which is enough to push many candidates below the local $v_{\rm esc}$. Five li2023 stars in the master have $\varpi < 0$; the Bailer-Jones catalogue gives them physically sensible distances of 2–5 kpc.

The main impact on the unbound classification is summarised in Table 2. *All counts in Table 2 are computed on the same final-strict sample of 356 stars; the two passes differ only in the distance estimator.* On this fixed sample, the count of likely-unbound stars ($P_{\rm unbound} > 0.5$) drops from 48 (inverse parallax) to 3 (Bailer-Jones), and the count of high-confidence unbound stars ($P_{\rm unbound} > 0.9$) drops from 12 to 1. Of the 48 stars classified as $P_{\rm unbound} > 0.5$ under inverse parallax, 45 are downgraded across the 0.5 threshold by the Bailer-Jones pass and 3 remain; no star is gained by switching estimators. The reduction is therefore not a side-effect of the LAMOST quality or RV-consistency cuts that define the final-strict sample, but a direct consequence of the choice of distance estimator.

4.3. Final kinematics

Figure 4 presents the Toomre diagram for the Gaia-only-clean (grey), final-strict (blue) and Top-3 (red star) populations under Bailer-Jones distances and Gaia radial velocities. The final-strict sample populates the halo-like region of the diagram, with typical $\sqrt{U^2 + W^2}$ in the range 200–400 km s^{-1}. Figure 5 expresses the same kinematics as the unbound ratio $v_{\rm grf}/v_{\rm esc}(R_{\rm gc})$ versus Bailer-Jones distance: the dashed horizontal line at $v_{\rm grf} = v_{\rm esc}$ is the unbound boundary, and only three stars from the final-strict sample sit at or above it.

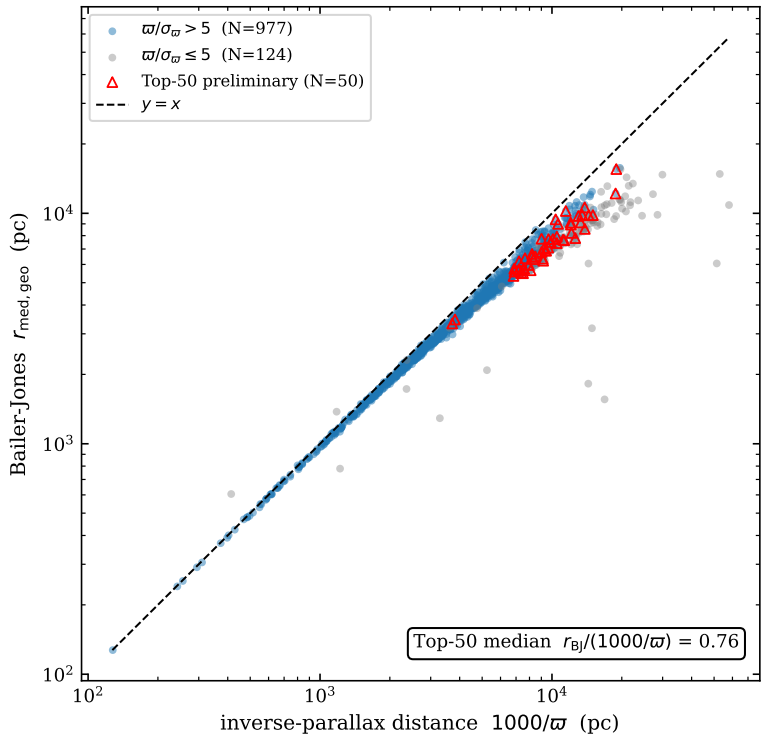

Figure 3. Pairwise comparison of inverse-parallax distances ($1000/\varpi$) and Bailer-Jones (2021) geometric distances ($r_{\mathrm{med,geo}}$). Triangles mark the 50 candidates with the largest preliminary P_{unbound}. Bailer-Jones distances are systematically smaller; the median ratio $r_{\mathrm{med,geo}}/(1000/\varpi)$ is 0.88 across the full 1101-star master sample and 0.76 on the preliminary Top-50.

4.4. Final candidate table

Figure 6 ranks the 30 final-strict candidates with the largest P_{unbound} (Top-30). The upper panel shows the Monte Carlo mean v_{grf} with $\pm 1\sigma$ error bars; the lower panel shows P_{unbound} with the rank-1, 2 and 3 candidates highlighted in red, orange and gold. Only 3 of 30 stars retain $P_{\mathrm{unbound}} > 0.5$ and a single star (rank 1) has $P_{\mathrm{unbound}} > 0.9$. Table 3 lists the Top-15 together with their LAMOST DR9 atmospheric parameters. The full Top-30 with the Monte Carlo dispersions, heliocentric $V_{\mathrm{tot,helio}}$, the per-star escape speed and Δv_{RV} is released as a machine-readable supplementary CSV (`tableA1_supplementary_top30.csv`).

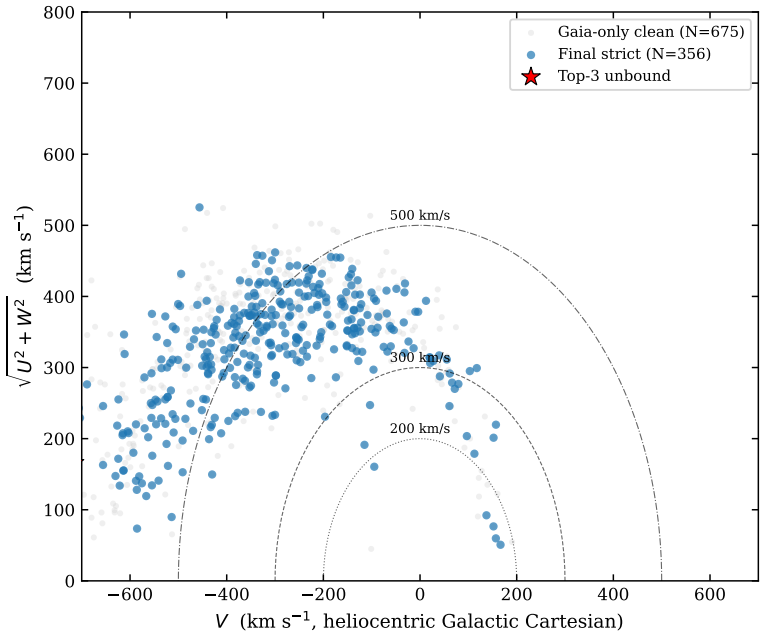

Figure 4. Toomre diagram showing $\sqrt{U^2 + W^2}$ versus V for the Gaia-only clean (grey), the final-strict sample (blue) and the highest-confidence Top-3 unbound candidates (red stars). The velocities are heliocentric Galactic Cartesian, with U positive toward the Galactic centre, V positive in the direction of Galactic rotation and W positive toward the North Galactic Pole; they are not LSR-corrected. Dashed circles mark constant heliocentric peculiar speeds of 200, 300 and 500 km s^{-1}.

4.5. Radial-velocity sensitivity

Figure 7 presents the radial-velocity sensitivity check on the final-strict sample. Per-star $v_{\rm grf}$ from Gaia DR3 and LAMOST DR9 radial velocities (panel a) lie almost exactly on the $y = x$ line; the distribution of the difference $\Delta v_{\rm grf}$ = LAMOST − Gaia (panel b) has median 0.00 km s^{-1}, $p_{90}|\Delta| = 5.7$ km s^{-1} and max $|\Delta| = 32.0$ km s^{-1}. Of the 356 final-strict stars only one flips $P_{\rm unbound}$ across the 0.5 threshold between the two RV passes. The LAMOST DR9 LRS radial velocities are known to carry an ≈ -5.7 km s^{-1} zero-point offset relative to Gaia DR3 in our matched subset; because we propagate uncertainties through the Monte Carlo, this offset does not propagate to a meaningful change in the main classification.

5. Discussion

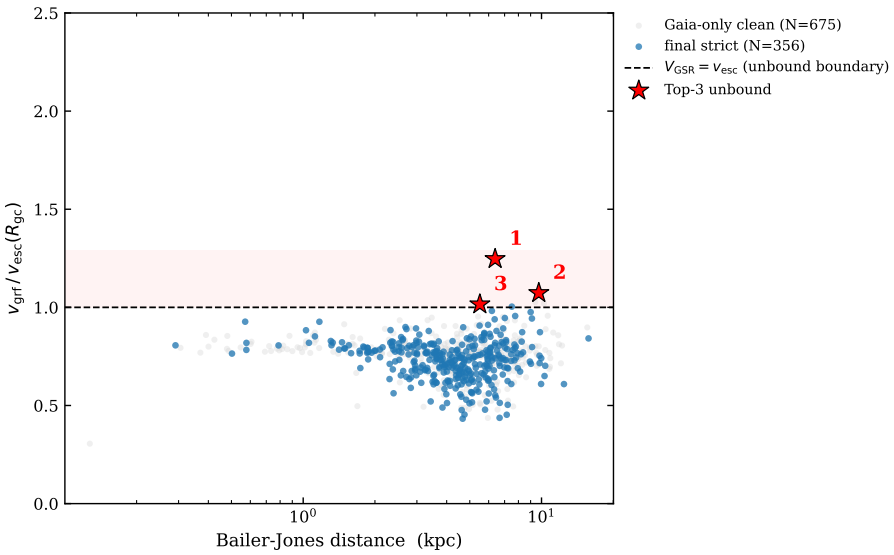

Figure 5. Ratio of the Galactocentric speed $v_{\rm grf}$ to the local escape speed $v_{\rm esc}(R_{\rm gc})$ under MWPotential2014, plotted against Bailer-Jones distance. The dashed horizontal line at $v_{\rm grf}/v_{\rm esc} = 1$ marks the unbound boundary; the lightly shaded region above it is the candidate-unbound zone. The Top-3 stars (red) are the only objects in the final-strict sample that sit close to or above this line.

5.1. Why most preliminary candidates are downgraded

The 24% median distance shrinkage of the Bailer-Jones estimator on the inverse-parallax-flagged unbound subset (Sect. 4.2) is sufficient to explain the same-sample drop from 48 to 3 stars with $P_{\rm unbound} > 0.5$. For tangentially dominated stars the inferred peculiar speed scales linearly with distance; combined with proper-motion uncertainties at the 0.05–0.5 mas yr^{-1} level a 24% distance reduction translates to $O(150\,{\rm km\,s^{-1}})$ change in $V_{\rm tot,helio}$, comparable to the $v_{\rm esc}$–$V_{\rm tot,helio}$ margin in the high-velocity tail. Our results are consistent with the Gaia-DR2-era reassessment of Boubert et al. (2018) and with the Gaia-DR2 fastest-stars analysis of Marchetti et al. (2019), both of which highlighted the strong dependence of unbound classifications on the distance prescription.

5.2. The Top-3 candidates

The three highest-confidence unbound candidates in the final strict sample are:

– **Rank 1**: Gaia DR3 source_id 1383279090527227264, present in both Li et al. (2021) and Liao et al. (2024); $d_{\rm BJ} = 6.39$ kpc, $\overline{v_{\rm grf}} = 653 \pm 55\,{\rm km\,s^{-1}}$,

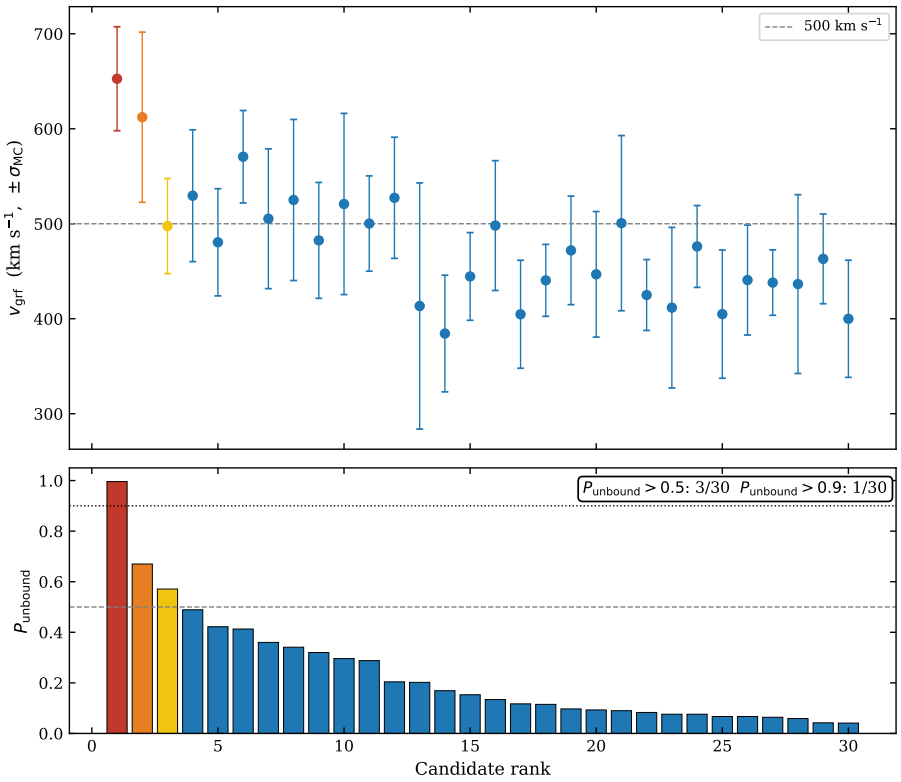

Figure 6. Top-30 final candidates ranked by P_{unbound}. *Top:* Monte Carlo mean v_{grf} with $\pm1\sigma$ error bars (1000 draws per star). *Bottom:* P_{unbound}, with the rank-1, 2 and 3 candidates highlighted in red, orange and gold. Reference lines: $P = 0.5$ (dashed), $P = 0.9$ (dotted), and $v_{\mathrm{grf}} = 500\,\mathrm{km\,s^{-1}}$ in the upper panel. After adopting Bailer-Jones geometric distances only 3/30 stars retain $P_{\mathrm{unbound}} > 0.5$ and 1/30 retains $P_{\mathrm{unbound}} > 0.9$, indicating that the unbound classification is highly sensitive to the choice of distance estimator.

$P_{\mathrm{unbound}} = 0.996$; LAMOST atmospheric parameters $T_{\mathrm{eff}} = 4801\,\mathrm{K}$, $\log g = 1.88$, $[\mathrm{Fe/H}] = -1.40$, i.e. a metal-poor giant. Independent inclusion in two literature catalogues lends support; recent chemical work on extreme-velocity stars (Nelson et al., 2024) provides relevant context for the population to which this object likely belongs.

– **Rank 2**: Gaia DR3 source_id `1204061267883975040` (liao2024 only), $d_{\mathrm{BJ}} = 9.74\,\mathrm{kpc}$, $\overline{v_{\mathrm{grf}}} = 612 \pm 90\,\mathrm{km\,s^{-1}}$, $P_{\mathrm{unbound}} = 0.670$; very metal-poor ($[\mathrm{Fe/H}] = -2.38$).

Table 3. Top-15 final high-velocity candidates ranked by $P_{\rm unbound}$. The full Top-30 with the Monte Carlo dispersions, heliocentric $V_{\rm tot,helio}$ and $\Delta v_{\rm RV}$ is released as a machine-readable supplementary CSV (`tableA1_supplementary_top30.csv`).

rank	Gaia DR3 source_id	catalogues	$d_{\rm BJ}$ [kpc]	$\overline{v_{\rm grf}}$ [km s^{-1}]	$P_{\rm unbound}$	$T_{\rm eff}$ [K]	$\log g$	[Fe/H]	notes
1	1383279090527227264	li2021,liao2024	6.39	653	0.996	4801	1.88	-1.40	high-confidence unbound; dual-catalogue
2	1204061267883975040	liao2024	9.74	612	0.670	4612	1.18	-2.38	likely unbound
3	3877058564258758656	liao2024	5.51	498	0.571	5143	2.29	-1.21	likely unbound
4	1375165725506487424	li2021,liao2024	7.51	530	0.489	4242	0.75	-1.29	dual-catalogue
5	2105847208541125248	liao2024	9.00	480	0.422	4507	1.08	-1.22	—
6	4450458649852400640	liao2024	6.19	571	0.413	4758	1.72	-1.59	—
7	1477675943342041472	liao2024	7.75	505	0.360	4799	1.67	-1.66	—
8	1297316350890352000	liao2024	9.11	525	0.341	4431	1.25	-1.23	—
9	3960007851762445696	li2021,liao2024	6.36	482	0.320	4928	2.13	-1.34	dual-catalogue
10	3651065597121243648	liao2024	5.50	521	0.296	5059	2.35	-2.11	—
11	1480182073940289024	liao2024	7.02	500	0.288	5667	3.54	-1.78	—
12	4429980078286167424	liao2024	5.97	527	0.204	4988	2.37	-1.67	—
13	3696393857329932672	liao2024	5.66	413	0.202	6523	4.29	-1.07	—
14	2125719266307162240	liao2024	15.75	384	0.169	4148	1.17	-0.73	—
15	1850497933774341504	liao2024	6.90	445	0.153	5595	3.13	-1.12	—

– **Rank 3**: Gaia DR3 source_id 3877058564258758656 (liao2024 only), $d_{\rm BJ} = 5.51$ kpc, $\overline{v_{\rm grf}} = 498 \pm 50$ km s^{-1}, $P_{\rm unbound} = 0.571$; metal-poor giant ($T_{\rm eff} = 5143$ K, $\log g = 2.29$, [Fe/H] $= -1.21$).

All three are giant or sub-giant late-type stars with metallicities typical of the Galactic halo, consistent with the late-type HVS candidate populations discussed by Li et al. (2020) and the Gaia–LAMOST high-velocity samples of Du et al. (2018a,b).

We checked the three sources against SIMBAD on 2026 April 30. Rank-1 is catalogued there as UCAC4 656-058031, with the SIMBAD position imported directly from Gaia DR3 (2020yCat.1350); rank-2 is present only as the Gaia DR3 entry itself; rank-3 has no SIMBAD record within 5 arcsec of its Gaia coordinates. None of the three carries a published variability, binarity or spectroscopic-binary flag at the time of writing. The only external corroboration we identify is the dual-catalogue inclusion of rank-1 in both Li et al. (2021) and Liao et al. (2024); this is also the only object in our sample with $P_{\rm unbound} > 0.9$. The absence of flags is, of course, not equivalent to a confirmation of single-star status: targeted multi-epoch spectroscopy of the kind reported by Hattori et al. (2019) for LAMOST-HVS1 remains the most direct test. We do not claim discovery; the Top-3 are reassessments of stars already present in the literature.

5.3. Gaia versus LAMOST radial velocities

The median difference LAMOST − Gaia $= -5.66$ km s^{-1} in the matched subset (Sect. 4.5) reflects the well-documented LAMOST DR9 LRS zero-point offset. We have not applied a zero-point correction in the primary kinematic solution, because the main classification is insensitive to it: the median $\Delta v_{\rm grf}$ on the

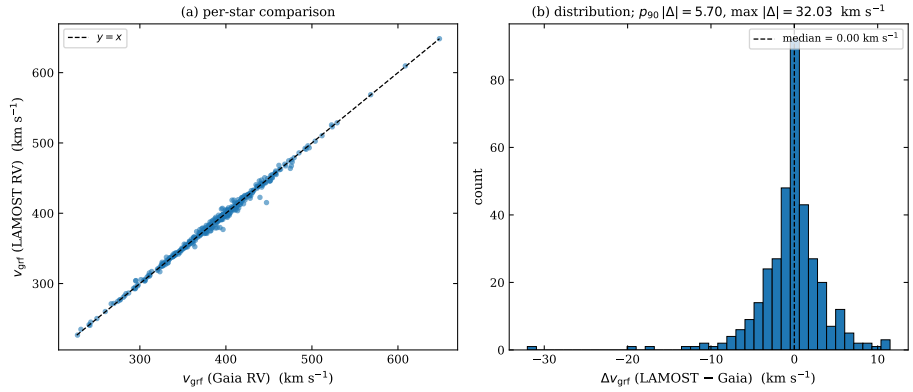

Figure 7. Radial-velocity sensitivity on the final-strict sample (N=356). *Panel (a):* per-star $v_{\rm grf}$ computed with Gaia DR3 radial velocities versus the same quantity computed with LAMOST DR9 radial velocities. *Panel (b):* histogram of the difference $\Delta v_{\rm grf}$ = LAMOST − Gaia; median = $0.00\,{\rm km\,s^{-1}}$, $p_{90}|\Delta| = 5.7\,{\rm km\,s^{-1}}$, $\max|\Delta| = 32.0\,{\rm km\,s^{-1}}$. The unbound classification is essentially insensitive to the choice of RV.

final-strict sample is $0.00\,{\rm km\,s^{-1}}$, the p_{90} absolute deviation is $5.7\,{\rm km\,s^{-1}}$, and the chemical tagging arguments of Hawkins & Wyse (2018) and Bromley et al. (2018) also do not require sub-km s^{-1} RV accuracy.

5.4. Limitations and follow-up

Four sources of systematic uncertainty affect the main numerical results. The first is the escape-speed approximation: $v_{\rm esc}$ is evaluated in the disk plane ($z = 0$), and off-plane corrections under MWPotential2014 are at the few-percent level. Because rank-2 and rank-3 sit close to the unbound boundary at $P_{\rm unbound} = 0.670$ and 0.571, their classification can flip under alternative potentials such as those of McMillan (2017) and Piffl et al. (2014); Monari et al. (2018). Only rank-1 ($P_{\rm unbound} = 0.996$) survives such variations as a robust unbound candidate; ranks 2 and 3 should be treated as marginal pending external confirmation. The second concerns the Bailer-Jones prior: it is tuned to the Galactic disk and may itself shrink the distances of genuine halo high-velocity tracers. The 48-to-3 reduction is therefore prior-dependent rather than a definitive measurement, and we phrase it that way throughout. The third systematic is sample geometry. LAMOST coverage is largely restricted to the northern hemisphere and the Li et al. (2023) subset contributes zero objects to the final-strict sample under our cross-match and quality criteria. Conclusions about atmospheric parameters therefore rest on the Li et al. (2021) and Liao et al. (2024) subsets only. The fourth is unresolved binarity: it can inflate the apparent radial velocity, and the

two stars with $|\Delta v_{\rm RV}| > 50\,{\rm km\,s^{-1}}$ that otherwise pass our quality gates are the natural targets for multi-epoch follow-up.

The follow-up programme implied by these results is therefore: (a) targeted high-resolution spectroscopy of the Top-3 candidates to confirm or refute their unbound status under a panel of Galactic potentials (e.g. McMillan, 2017; Piffl et al., 2014; Monari et al., 2018); (b) multi-epoch radial-velocity monitoring of the two RV-outlier follow-up targets; and (c) re-running the present pipeline with Gaia DR4 parallaxes once they become available—we expect the parallax error budget to halve and the BJ-vs-inverse-parallax distance gap to narrow.

6. Conclusions

1. For the 356-star final-strict subset of three published HVS catalogues (Li et al., 2021, 2023; Liao et al., 2024), replacing inverse-parallax distances with Bailer-Jones geometric distances reduces the count of likely-unbound stars ($P_{\rm unbound} > 0.5$) from *48* to *3* and the count of high-confidence unbound stars ($P_{\rm unbound} > 0.9$) from *12* to *1*. 45 stars are downgraded across $P_{\rm unbound} = 0.5$ and none are promoted.

2. The reduction is driven by a systematic distance shrinkage of 12 % across the strict sample, rising to 24 % on the subset that the inverse-parallax pass had flagged as $P_{\rm unbound} > 0.5$. Substituting LAMOST radial velocities for Gaia radial velocities on the same sample changes the median $v_{\rm grf}$ by $0\,{\rm km\,s^{-1}}$ ($p_{90}|\Delta| = 5.7\,{\rm km\,s^{-1}}$) and flips the $P_{\rm unbound} = 0.5$ classification of only one star. The unbound classification is therefore distance-dominated, not RV-dominated.

3. We release a final-strict sample of 356 stars, a Top-15 main candidate table (Table 3) and a supplementary Top-30 as a machine-readable CSV. The three highest-confidence candidates are the metal-poor giants Gaia DR3 `1383279090527227264`, `1204061267883975040` and `3877058564258758656`; targeted spectroscopic follow-up is recommended.

4. Two stars with $|\Delta_{\rm rv}\,({\rm LAMOST} - {\rm Gaia})| > 50\,{\rm km\,s^{-1}}$ are flagged as binary or variable-RV candidates; we do not include them in the principal unbound list and report them separately as follow-up targets.

All raw queries, the kinematic solver, the figure- and table-generation scripts and the unit tests are publicly available at `https://github.com/Harry33t/caosp-hivel-pipeline` under the MIT license. A versioned snapshot will be assigned a permanent DOI upon acceptance. The Top-30 machine-readable supplementary CSV is included with the submission package.

Acknowledgements

We thank the anonymous referee whose detailed comments substantially improved the robustness analysis and the presentation of this work. This work has made use of data from the European Space Agency mission *Gaia* (https://www.cosmos.esa.int/gaia), processed by the *Gaia* Data Processing and Analysis Consortium. Funding for the DPAC has been provided by national institutions, in particular the institutions participating in the *Gaia* Multilateral Agreement. Guoshoujing Telescope (LAMOST) is a National Major Scientific Project built by the Chinese Academy of Sciences. This research has made use of the VizieR catalogue access tool, CDS, Strasbourg, France (Ochsenbein et al., 2000). Software: `astropy` (Astropy Collaboration et al., 2013, 2018), `astroquery` (Ginsburg et al., 2019), `galpy` (Bovy, 2015).

References

Astropy Collaboration, Price-Whelan, A. M., Sipőcz, B. M., et al., The Astropy Project: Building an Open-science Project and Status of the v2.0 Core Package. 2018, *Astronomical Journal*, **156**, 123, DOI:10.3847/1538-3881/aabc4f

Astropy Collaboration, Robitaille, T. P., Tollerud, E. J., et al., Astropy: A community Python package for astronomy. 2013, *Astronomy and Astrophysics*, **558**, A33, DOI:10.1051/0004-6361/201322068

Bailer-Jones, C. A. L., Estimating Distances from Parallaxes. 2015, *Publications of the ASP*, **127**, 994, DOI:10.1086/683116

Bailer-Jones, C. A. L., Rybizki, J., Fouesneau, M., Demleitner, M., & Andrae, R., Estimating Distances from Parallaxes. V. Geometric and Photogeometric Distances to 1.47 Billion Stars in Gaia EDR3. 2021, *Astronomical Journal*, **161**, 147, DOI:10.3847/1538-3881/abd806

Bennett, M. & Bovy, J., Vertical waves in the solar neighbourhood in Gaia DR2. 2019, *Monthly Notices of the RAS*, **482**, 1417, DOI:10.1093/mnras/sty2813

Boubert, D., Guillochon, J., Hawkins, K., et al., Revisiting hypervelocity stars after Gaia DR2. 2018, *Monthly Notices of the RAS*, **479**, 2789, DOI:10.1093/mnras/sty1601

Bovy, J., galpy: A python Library for Galactic Dynamics. 2015, *Astrophysical Journal, Supplement*, **216**, 29, DOI:10.1088/0067-0049/216/2/29

Bromley, B. C., Kenyon, S. J., Brown, W. R., & Geller, M. J., Nearby High-speed Stars in Gaia DR2. 2018, *Astrophysical Journal*, **868**, 25, DOI:10.3847/1538-4357/aae83e

Brown, W. R., Hypervelocity Stars. 2015, *Annual Review of Astron and Astrophys*, **53**, 15, DOI:10.1146/annurev-astro-082214-122230

Brown, W. R., Geller, M. J., & Kenyon, S. J., The MMT Hypervelocity Star Survey. III. The Complete Survey. 2014, *Astrophysical Journal*, **787**, 89, DOI:10.1088/0004-637X/787/1/89

Brown, W. R., Geller, M. J., Kenyon, S. J., & Kurtz, M. J., Discovery of an Unbound Hypervelocity Star in the Milky Way Halo. 2005, *Astrophysical Journal, Letters*, **622**, L33, DOI:10.1086/429378

Brown, W. R., Geller, M. J., Kenyon, S. J., & Kurtz, M. J., Hypervelocity Stars. II. The Bound Population. 2007, *Astrophysical Journal*, **660**, 311, DOI:10.1086/513595

Cui, X.-Q., Zhao, Y.-H., Chu, Y.-Q., et al., The Large Sky Area Multi-Object Fiber Spectroscopic Telescope (LAMOST). 2012, *Research in Astronomy and Astrophysics*, **12**, 1197, DOI:10.1088/1674-4527/12/9/003

Deng, L.-C., Newberg, H. J., Liu, C., et al., LAMOST Experiment for Galactic Understanding and Exploration (LEGUE)—The Survey's Science Plan. 2012, *Research in Astronomy and Astrophysics*, **12**, 735, DOI:10.1088/1674-4527/12/7/003

Du, C., Li, H., Liu, S., Donlon, T., & Newberg, H. J., The High-velocity Stars in the Local Stellar Halo from Gaia and LAMOST. 2018a, *Astrophysical Journal*, **863**, 87, DOI:10.3847/1538-4357/aad088

Du, C., Li, H., Yan, Y., et al., The Origin of High-velocity Stars Considering the Impact of the Galactic Bar. 2018b, *Astrophysical Journal, Letters*, **869**, L31, DOI:10.3847/2041-8213/aaf578

Elsanhoury, W. H., Kinematics of high-velocity stars utilizing LAMOST and Gaia DR3 archives within 100 kpc. 2025, *Contributions of the Astronomical Observatory Skalnaté Pleso*, **55**, 38, DOI:10.31577/caosp.2025.55.1.38

Gaia Collaboration, Vallenari, A., Brown, A. G. A., et al., Gaia Data Release 3: Summary of the content and survey properties. 2023, *Astronomy and Astrophysics*, **674**, A1, DOI:10.1051/0004-6361/202243940

Ginsburg, A., Sipőcz, B. M., Brasseur, C. E., et al., astroquery: An Astronomical Web-querying Package in Python. 2019, *Astronomical Journal*, **157**, 98, DOI:10.3847/1538-3881/aafc33

Gravity Collaboration, Abuter, R., Amorim, A., Anugu, N., et al., Detection of the gravitational redshift in the orbit of the star S2 near the Galactic centre massive black hole. 2018, *Astronomy and Astrophysics*, **615**, L15, DOI:10.1051/0004-6361/201833718

Hattori, K., Valluri, M., Castro, N., et al., Origin of a Massive Hyper-runaway Subgiant Star LAMOST-HVS1: Implication from Gaia and Follow-up Spectroscopy. 2019, *Astrophysical Journal*, **873**, 116, DOI:10.3847/1538-4357/ab05c8

Hawkins, K. & Wyse, R. F. G., The fastest travel together: chemical tagging of the fastest stars in Gaia DR2 to globular clusters. 2018, *Monthly Notices of the RAS*, **481**, 1028, DOI:10.1093/mnras/sty2282

Hills, J. G., Hyper-velocity and tidal stars from binaries disrupted by a massive Galactic black hole. 1988, *Nature*, **331**, 687, DOI:10.1038/331687a0

Kenyon, S. J., Bromley, B. C., Geller, M. J., & Brown, W. R., Hypervelocity Stars: From the Galactic Center to the Halo. 2008, *Astrophysical Journal*, **680**, 312, DOI:10.1086/587738

Li, J., Liu, C., Xue, X.-X., et al., Three new late-type hypervelocity star candidates from SDSS, LAMOST and Gaia. 2020, *Research in Astronomy and Astrophysics*, **20**, 42, DOI:10.1088/1674-4527/20/3/42

Li, Q.-Z., Lu, Y.-J., Yang, T.-G., Qiu, K.-N., & Liao, J., On the Origins of Extreme Velocity Stars as Revealed by Large-scale Galactic Surveys. 2023, *Astronomical Journal*, **166**, 12, DOI:10.3847/1538-3881/acd1dc

Li, Y.-B., Luo, A.-L., Lu, Y.-J., et al., 591 High-velocity Stars in the Galactic Halo Selected from LAMOST DR7 and Gaia DR2. 2021, *Astrophysical Journal, Supplement*, **252**, 3, DOI:10.3847/1538-4365/abc16e

Liao, J., Lu, Y.-J., Mu, H.-J., & Yang, T.-G., The Origin of High-velocity Stars Considering the Impact of the Large Magellanic Cloud. 2024, *Astronomical Journal*, **167**, 76, DOI:10.3847/1538-3881/ad18c4

Lindegren, L., Bastian, U., Biermann, M., et al., Gaia Early Data Release 3. Parallax bias versus magnitude, colour, and position. 2021, *Astronomy and Astrophysics*, **649**, A4, DOI:10.1051/0004-6361/202039653

Luri, X., Brown, A. G. A., Sarro, L. M., et al., Gaia Data Release 2. Using Gaia parallaxes. 2018, *Astronomy and Astrophysics*, **616**, A9, DOI:10.1051/0004-6361/201832964

Marchetti, T., Rossi, E. M., & Brown, A. G. A., Gaia DR2 in 6D: searching for the fastest stars in the Galaxy. 2019, *Monthly Notices of the RAS*, **490**, 157, DOI:10.1093/mnras/sty2592

McMillan, P. J., The mass distribution and gravitational potential of the Milky Way. 2017, *Monthly Notices of the RAS*, **465**, 76, DOI:10.1093/mnras/stw2759

Monari, G., Famaey, B., Carrillo, I., et al., The escape speed curve of the Galaxy obtained from Gaia DR2 implies a heavy Milky Way. 2018, *Astronomy and Astrophysics*, **616**, L9, DOI:10.1051/0004-6361/201833748

Nelson, T., Ting, Y.-S., Hawkins, K., et al., A detailed chemical study of the extreme velocity stars in the Galaxy. 2024, *Monthly Notices of the RAS*, **532**, 2875, DOI:10.1093/mnras/stae1656

Ochsenbein, F., Bauer, P., & Marcout, J., The VizieR database of astronomical catalogues. 2000, *Astronomy and Astrophysics, Supplement*, **143**, 23, DOI:10.26093/cds/vizier

Piffl, T., Scannapieco, C., Binney, J., et al., The RAVE survey: the Galactic escape speed and the mass of the Milky Way. 2014, *Astronomy and Astrophysics*, **562**, A91, DOI:10.1051/0004-6361/201322531

Reid, M. J. & Brunthaler, A., The Proper Motion of Sagittarius A*. III. The Case for a Supermassive Black Hole. 2020, *Astrophysical Journal*, **892**, 39, DOI:10.3847/1538-4357/ab76cd

Schönrich, R., Binney, J., & Dehnen, W., Local kinematics and the local standard of rest. 2010, *Monthly Notices of the RAS*, **403**, 1829, DOI:10.1111/j.1365-2966.2010.16253.x

Xiang, M.-S., Liu, X.-W., Yuan, H.-B., et al., The LAMOST stellar parameter pipeline at Peking University – LSP3. 2015, *Monthly Notices of the RAS*, **448**, 822, DOI:10.1093/mnras/stu2692

Yan, H.-L., Zhou, Y.-T., Zhang, X., et al., Overview of the LAMOST survey in the first decade. 2022, *The Innovation*, **3**, 100224, DOI:10.1016/j.xinn.2022.100224

Yu, Q. & Tremaine, S., Ejection of Hypervelocity Stars by the (Binary) Black Hole in the Galactic Center. 2003, *Astrophysical Journal*, **599**, 1129, DOI:10.1086/379546

Zhao, G., Zhao, Y.-H., Chu, Y.-Q., Jing, Y.-P., & Deng, L.-C., LAMOST spectral survey – An overview. 2012, *Research in Astronomy and Astrophysics*, **12**, 723, DOI:10.1088/1674-4527/12/7/002